

Relationship Between the Microstructure/Pore Structure of Oil-Well Cement and Hydrostatic Pressure

Kaiqiang Liu¹ · Xiaowei Cheng¹ · Xingguo Zhang² · Zaoyuan Li² · Jia Zhuang¹ · Xiaoyang Guo²

Received: 8 September 2017 / Accepted: 26 April 2018 / Published online: 8 May 2018
© Springer Science+Business Media B.V., part of Springer Nature 2018

Abstract In cementing operations, hydrostatic pressure reduction in cement slurries is a serious threat to operation safety and cementing quality. This study combines X-ray diffraction, thermogravimetric analysis, scanning electron microscopy, low-field nuclear magnetic resonance, and nano-computed tomography to investigate the mechanism of hydrostatic pressure reduction in cement slurries. The experimental results reveal that hydrostatic pressure transmission in a fresh cement slurry follows Pascal's law. However, in the slurry, some cement particles undergo sedimentation with an increase in the hydration time, which reduces a part of the hydrostatic pressure. Further, another part of the hydrostatic pressure, which is maintained by the free water in the slurry pores, is reduced during the hardening stage. When the hydration reaction of the slurry is accelerated, the pore water in the slurry is supersaturated and hydration products start to rapidly nucleate and grow between the cement particles. These hydration products are porous gel structures and can change the pore structure of the cement slurry; a macro-pore is divided into many micropores, such as capillary pores and gel pores. Because these pores are filled by water in the slurry, during this process, free water in the macro-pores is changed to capillary water and gel water. However, gel water and capillary water cannot transmit hydrostatic pressure in the cement slurry. Meanwhile, in the fresh cement slurry, many pores containing free water are connected and some hydration products rapidly grow in the macro-pores and fill them, which may reduce the column height of the free water in the pores and lead to hydrostatic pressure reduction in the slurry.

Keywords Hydrostatic pressure · Oil-well cement · Microstructure · Pore structure · Pore water distribution

✉ Xiaowei Cheng
chengxw@swpu.edu.cn; zj-656@163.com

¹ School of Material Science and Engineering, Southwest Petroleum University, Chengdu, China

² Key Laboratory of Oil and Gas Reservoir Geology and Exploration, Southwest Petroleum University, Chengdu, China

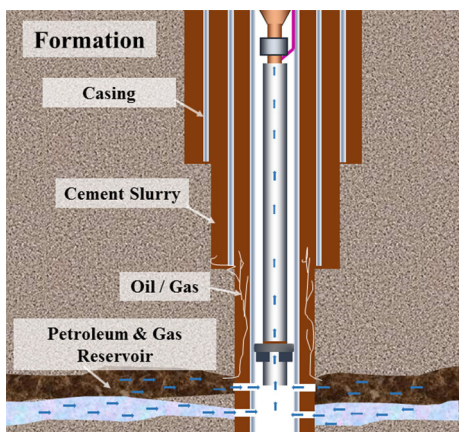
1 Introduction

In petroleum engineering, the depth of oil and natural gas wells is generally of the order of a few kilometres and oil-well cement slurries are used to isolate the rock formations a few kilometres below the ground level. Suitable density, thickening time, and rheological properties of the cement slurry are required to form a hydraulic seal in the annulus between the well-face and casing (Baumgarte et al. 1999); uncontrolled migration of oil/gas in the annulus space between the casing and formation should be avoided in the well. However, cement is a cementitious material; its hydrostatic pressure is reduced in the early hardening stages (Carter and Slagle 1972; Dusterhoff et al. 2002; Newman et al. 2001), which causes pressure imbalance between oil/gas and the cement slurry and leads to oil/gas migration into the hardening cement slurry. This may even lead to serious accidents, such as a blowout (Dusterhoff et al. 2002). Figure 1 schematically depicts an oil/gas migration scenario. Moreover, the migration process may destroy the properties and microstructure of the cement slurry, which threatens cementing quality and safety.

Currently, there are several reports and theories on hydrostatic pressure reduction in cement slurries, of which the shear stress theory proposed by Sutton (Li et al. 2016; Sutton et al. 1984) is the most widely accepted theory. This theory suggests a quantitative evaluation of the shear stress between cement particles by testing the static gel strength of a cement slurry. Moreover, it was observed that increase in the shear stress of a cement slurry follows a linear relationship with a decrease in the hydrostatic pressure. Meanwhile, Sabins and Services (1982) investigated property evolution in a cement slurry during hydrostatic pressure reduction. Zhang (2002) conducted extensive research on hydrostatic pressure reduction in cement slurries in the early hardening stage and evaluated their rheological properties, static gel strength, and other properties. However, these studies are limited to the relationship between the macro-properties of a cement slurry, borehole size, and hydrostatic pressure reduction; there is little literature available on the microstructure and properties of cement slurries during the hydrostatic pressure reduction stage.

Owing to the development of testing technology, some methods, such as low-field nuclear magnetic resonance (LF-NMR) and X-ray computed tomography (CT), are being widely used for studying the microstructure of cement materials (Bede et al. 2016; Chung et al. 2016; Ji et al. 2015; Kim et al. 2012; Marchon and Flatt 2015; Schock et al. 2016). LF-

Fig. 1 Schematic illustration of oil/gas migration into the hardening cement slurry



NMR can effectively detect the pore structure by analysing water distribution in cement materials (Dallas et al. 2014; Skibsted and Andersen 2013). Bede et al. (2016) and McDonald et al. (2010) analysed cement pastes by LF-NMR and found that the peak of the transverse relaxation time (T_2) ($0.1 \text{ ms} < T_2 < 1.2 \text{ ms}$) is generated by water in the intra- and inter-C–S–H gel pores and named the water present in the gel pores ‘gel water.’ The peak, $1.5 \text{ ms} < T_2 < 7.5 \text{ ms}$, is generated by water in the capillary pores, which is named as the capillary water; the peak, $7.5 \text{ ms} < T_2$, is generated by free water. Meanwhile, CT has been used for the quantitative analysis of porosity and pore structure of cement materials (Bernardes et al. 2015; Hou et al. 2017; Lanzón et al. 2012). In this study, we combined X-ray diffraction (XRD) analysis and thermogravimetric analysis (TG) to investigate the hydration rate and phase changes during hydrostatic pressure reduction in a cement slurry. LF-NMR, scanning electron microscopy (SEM), and nano-computed tomography (nano-CT) are used together for testing the pore structure, pore water distribution, and microstructure of the cement slurry. Further, the hydrostatic pressure reduction mechanism in cement slurries is studied.

2 Materials and Methods

2.1 Materials and Preparation of Samples

G-class oil-well cement is widely used in the cementing operations of oil and natural gas wells. It is obtained by grinding a Portland cement clinker, and in this study, it was produced according to the API 10-A specifications (American Petroleum Institute (API) 2002) at Sichuan Jiahua Co., Ltd. Figure 2 shows the XRD pattern and particle size distribution of the G-class oil-well cement used in this study. The main chemical components of the oil-well cement were tested by X-ray fluorescence (XRF). The mass percentages of the main chemical components are $m(\text{CaO})=61.799 \text{ wt\%}$, $m(\text{SiO}_2)=20.382 \text{ wt\%}$, $m(\text{Al}_2\text{O}_3)=3.370 \text{ wt\%}$, $m(\text{Fe}_2\text{O}_3)=4.152 \text{ wt\%}$, $m(\text{SO}_3)=4.711 \text{ wt\%}$, $m(\text{MgO})=1.951 \text{ wt\%}$, $m(\text{K}_2\text{O})=0.444 \text{ wt\%}$, and $m(\text{Na}_2\text{O})=0.359 \text{ wt\%}$. The filtrate reducer consists of a 2-acrylamido-2-methylpropanesulfonic acid/acrylamide/acrylic acid (AMPS/AM/AA) terpolymer and the dispersant contains an acetone and formaldehyde condensation polymer; they were supplied by Beijing Oilchemleader Science & Technology Development Co., Ltd. The cement slurry formulations used in the current investigation are listed in Table 1.

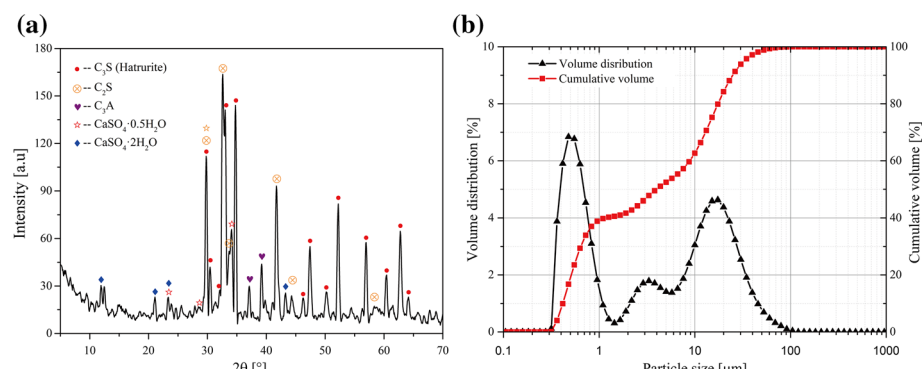


Fig. 2 **a** X-ray diffraction analysis and **b** particle size distribution of G-class oil-well cement

Table 1 Formulations of cement slurry specimens

ID	Cement/wt%	Filtrate reducer/wt%	Dispersant/wt%	Water/wt%	Water-to-cement ratio (W/C)
1#	100	0	0.1	44	0.44
2#	100	2	0.1	44	0.44

2.2 Experimental Procedure

2.2.1 Conventional Property Analysis

In accordance with the API standards (American Petroleum Institute (API) 2013), the cement slurry is mixed and its density, stability, and rheological properties are evaluated. A coquette viscometer is used to measure the rheological properties of the cement slurry. The slurry is a power law fluid, and two parameters, the behaviour index (n) and consistency index (k), are used to describe it. The two parameters, n and k , are calculated according to Eq. (1).

$$\tau = k \times \gamma^n \quad (1)$$

Here τ is the shear stress expressed in Pa, γ is the shear rate expressed in s^{-1} , n is the behaviour index of the slurry, which is dimensionless, and k is the consistency index of the slurry, expressed in Pa s.

The sedimentation stability of a cement slurry is a key parameter to evaluate whether the slurry experiences particle sedimentation. Particle sedimentation can lead to free fluids and density inhomogeneity in the cement slurry. To analyse these characteristics, we conducted the free fluid test and sedimentation test (American Petroleum Institute (API) 2013). In the free fluid test, a clear 250-mL glass cylinder was used; the slurry is poured into the cylinder up to the 250-mL mark; and a 2-h test period is initiated at 30 °C. After 2 h, the volume of the free fluid is measured and its volume fraction is calculated. Meanwhile, in the sedimentation test, a sedimentation tube (inner diameter 25 ± 0.5 mm, tube length 100 mm) is used. The slurry is injected into the tube and cured at 30 °C. After setting, the specimen is removed from the tube and divided into three equal segments from bottom to top. The density of each segment is tested according to Archimedes' principle.

2.2.2 Hydrostatic Pressure Testing

Figure 3 shows the general assembly drawing and diagram of a hydrostatic pressure testing device. The device includes a detachable vessel, simulated casing, temperature control system, pressure measurement system, and computer system. The detachable vessel has an inner diameter of 80 mm, and its vessel height is 1000 mm. The simulated casing has a diameter of 40 mm. The experimental procedure for hydrostatic pressure testing includes the following steps.

- (1) Initially, the hydrostatic pressure testing device is assembled and the vessel temperature is controlled at 30 °C using a computer system and temperature control system.
- (2) In the second step, the cement slurry is poured into the annulus between the vessel and simulated casing; the slurry is puddled to dislodge any air bubbles; and the vessel is filled completely.

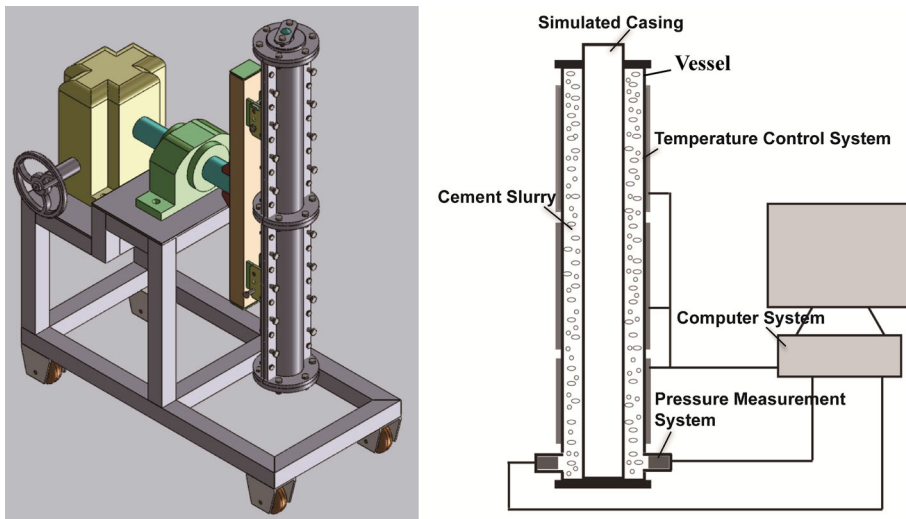


Fig. 3 General assembly drawing and diagram of a hydrostatic pressure testing device

- (3) The hydration temperature of the cement slurry is maintained at 30 °C.
- (4) After every 30 s, the hydrostatic pressure of the cement slurry is recorded using the computer system; this process was continued until the hydrostatic pressure decreased to zero.

2.2.3 Hydration Rate Testing of the Cement Slurry

The G-class oil-well cement is a Portland cement and mainly contains dicalcium silicate (C_2S) and tricalcium silicate (C_3S) (Joseph et al. 2017). Calcium hydroxide (CH) is one of the major hydration products. At about 450 °C, CH breaks down into calcium oxide (CaO) and water (H_2O) and water falls away from the specimen to reduce specimen weight (Angulo-Ramírez et al. 2017; Lothenbach et al. 2007). Therefore, TG is usually conducted to quantify the CH content of cement slurries and analyse the hydration reaction rate. In this study, specimens hydrated for specific time periods are dried by liquid nitrogen freezing and vacuum drying, after which their CH contents are tested by TG. The heating rate during the TG experiment is set at 10 °C/min. From the obtained results, the decomposition temperature of CH is determined to be in the range of 410–460 °C.

2.2.4 Microstructure Analysis Using SEM and Nano-CT

The evolution of microstructure in the cement slurry during liquid–solid transition is investigated using SEM. The tested cement slurries are prepared according to the API standards (American Petroleum Institute (API) 2013). The cement slurries are injected into a plastic pipe (inner diameter of 5 mm and length of 75 mm) and cured at a temperature less than 30 °C. After these samples are cured for preset time intervals, liquid nitrogen and vacuum freeze-drying technologies are used to stagnate the hydration of the cement slurries. Finally, a thin layer of gold is sprayed on the surfaces of the dried samples for SEM observation.

Nano-computed tomography was conducted on an instrument manufactured by GE Sensing & Inspection Technologies GmbH, Germany. Its minimum resolution is 0.2 μm ; it can be

used for observing the evolution of cement particles and pores in the cement slurry. Before starting the experiment, the indoor temperature is maintained at 30 °C. The prepared cement slurry is injected into a plastic pipe with an inner diameter of 5 mm and length of 75 mm to obtain the nano-CT sample. The prepared sample is fixed in the nano-CT sample table, which is then adjusted to observe the bottom of the sample. In order to ensure clarity of the experimental results, during the nano-CT scanning process, the rotation rate of the sample table is maintained at 36°/min. During the entire testing cycle, the sample is immobile and the evolution of the internal 3D microstructure of the cement slurry is analysed at different hydration times.

2.2.5 LF-NMR Testing

The LF-NMR technique is mainly used to test the T_2 values of the specimens. The interaction between water molecules and pore surfaces is a major factor affecting T_2 [also known as surface relaxation time (T_{2s})]. An important feature of T_{2s} is that the relaxation time of pore water is related to the surface area of the pores; therefore, T_2 can be calculated according to Eq. (2).

$$\frac{1}{T_2} = \frac{1}{T_{2s}} = \rho_2 \frac{S_i}{V_i} \quad (2)$$

Here T_2 is the transverse relaxation time, T_{2s} is the surface relaxation time, V_i is the pore volume, and S_i is the surface area of the pores.

A cement slurry is a porous material; in a fresh cement slurry, the pores are filled with water. In order to explore the hydrostatic pressure reduction mechanism in cement slurries, LF-NMR (Shanghai Niumag Company Ltd.) testing is carried out to analyse the changes in water distribution in the cement slurry during the hardening process. The experimental procedure includes the following steps. The prepared cement slurry is injected into a glass tube with an inner diameter of 19 mm, and the hydration temperature is maintained at 30 °C.

3 Results and Discussion

3.1 Hydrostatic Pressure Analysis

Figure 4 shows the hydrostatic pressure curves of 1# and 2# cement slurries and water. According to the device parameters (as shown in Fig. 3) and the tested hydrostatic pressure of water (as shown in Fig. 4), we can decipher that the accuracy rate of the pressure measurement system is about 95%. Based on the parameters shown in Table 2 and Pascal's law, the theoretical hydrostatic pressure of 1# and 2# slurries is 19 kPa and the tested initial value is about 18 kPa. It can be found that the transmission of initial hydrostatic pressure in fresh 1# and 2# follows Pascal's law and the curves can be divided into 3 stages. There is a distinct difference between the hydrostatic pressures of 1# and 2# in stage I. With an increase in the hydration time, the changes in the hydrostatic pressure curves are similar in stages II and III; the only difference is that the hydrostatic pressure reduction rate of 1# is faster than that of 2# in stage III.

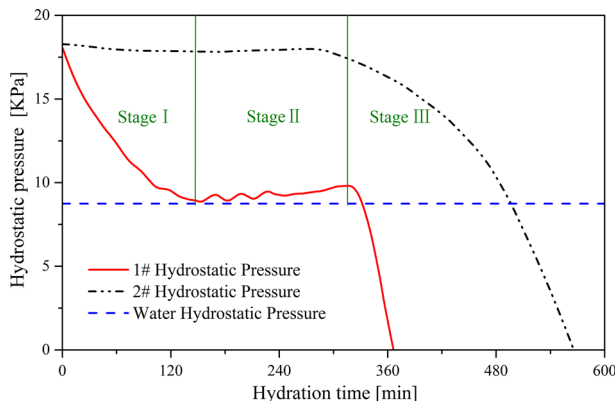


Fig. 4 Hydrostatic pressures of cement slurries 1#, 2#, and water

Table 2 Conventional properties of cement slurries

ID	Density/(g/cm ³) <i>n</i>	<i>k</i> /(Pa s)	Free fluid/%	Stability/(g/cm ³)			
				Top segment	Middle segment	Bottom segment	
1#	1.90	0.78	2.75	0.80	1.87	1.91	1.92
2#	1.90	0.73	4.47	0.00	1.90	1.90	1.90

3.2 Analysis of Conventional Properties

To study the differences in the hydrostatic pressures of 1# and 2# in stage I, the conventional properties and microstructures of the cement slurries are evaluated. The results are listed in Table 2, Figs. 5 and 6. In 1#, a free fluid phenomenon and density inhomogeneity can be observed. On the other hand, 2# does not exhibit this phenomenon. Therefore, it can be stated that the stability of 2# is better than that of 1#. From the microstructures (shown in Fig. 6), it can be seen that the internal microstructures of 1# and 2# are different. In 1#, the particles are in contact with each other and accumulate tightly (Li et al. 2016; Prohaska et al. 1993); this can be explained in terms of localized bridging or sedimentation of cement suspensions. In 2#, the particles are suspended by a net structure. With respect to the formulations of the tested cement slurries (shown in Table 1), the net structure is formed by a filtrate reducer. The net structure inhibits cement particle sedimentation and increases the stability of 2# (as shown in Table 2). Thus, the gravity force of cement particles in 2# can be transmitted by hydrostatic pressure early on in the hydration stage. Therefore, in stage I, the main reason for hydrostatic pressure reduction in 1# may be particle sedimentation. Hydrostatic pressure cannot transmit the gravity force of sediment particles, due to which the hydrostatic pressure of 1# in stage II is approximately equal to the hydrostatic pressure of water.

3.3 Hydration Rates of the Cement Slurries

The changes in the hydrostatic pressure curves of 1# and 2# are similar in stage III, but the change in the hydration rate of 1# is faster than that in 2#. To analyse this phenomenon,

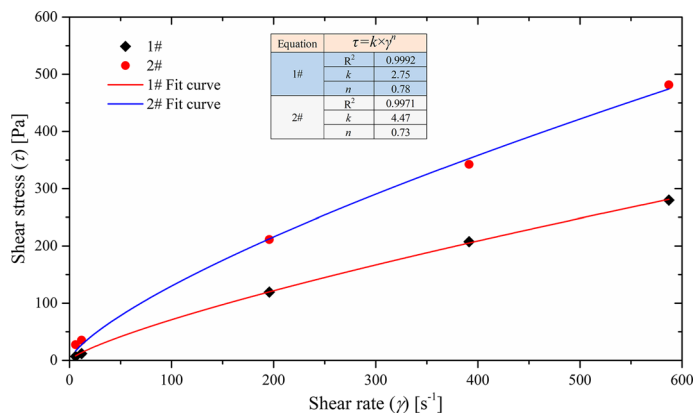


Fig. 5 Rheological properties of 1# and 2# cement slurries

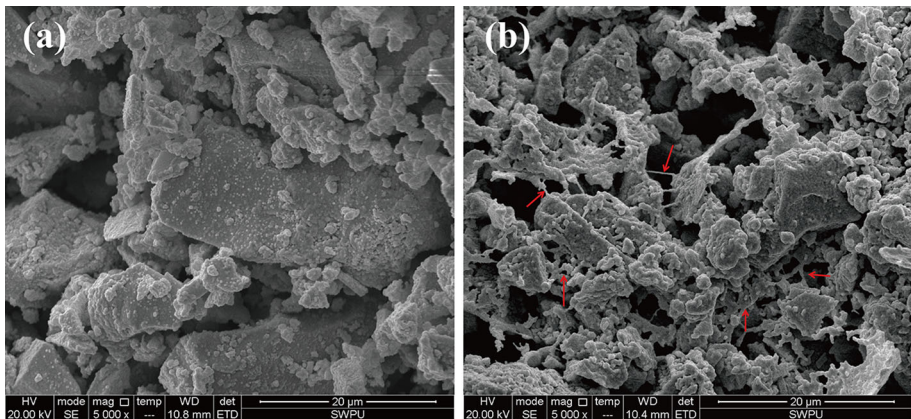


Fig. 6 Microstructures of cement slurries after hydration for 120 min. **a** 1# and **b** 2#

the Ca(OH)_2 contents of 1# and 2# at different hydration times are evaluated. Ca(OH)_2 is a major hydration product, and its content represents the hydration rate of a cement slurry. Figure 7 shows the TG results of Ca(OH)_2 analysis of 1# and 2#. It can be observed that the Ca(OH)_2 content in 1# and 2# rapidly increased in stage III; further, the rate of increase in 1# is higher than that in 2#. Therefore, it can be suggested that the hydration reaction rate of cement slurries rapidly increases in stage III and that the hydration reaction rate of 1# is faster than that of 2#. From these observations, it can also be inferred that hydrostatic pressure reduction is closely related to the hydration reaction rate of a cement slurry.

For an in-depth analysis of the hydrostatic pressure reduction mechanism in 1#, its microstructure evolution, pore structure, and water distribution at hydrostatic pressure reduction stage are studied by nano-CT, SEM, and LF-NMR.

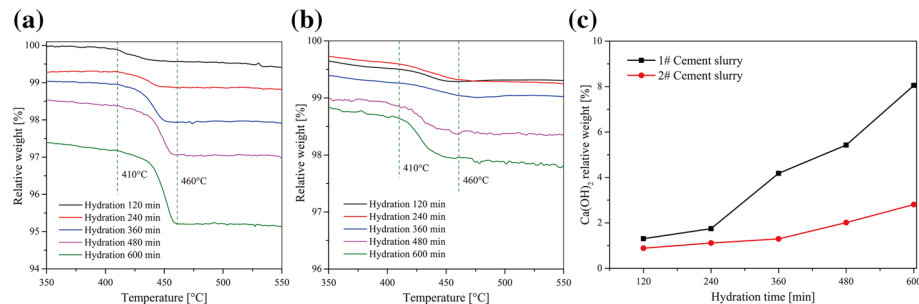


Fig. 7 $\text{Ca}(\text{OH})_2$ relative weight test results using TG. **a** TG curve of 1#, **b** TG curve of 2#, and **c** $\text{Ca}(\text{OH})_2$ relative weights

3.4 Relationship Between Hydrostatic Pressure and Microstructure

3.4.1 Nano-CT Analysis of the Three-Dimensional Microstructure of 1#

Rapid hydration of a cement slurry leads to a rapid microstructural evolution. Figure 8 presents the three-dimensional (3D) microstructure of 1#, as analysed by nano-CT. Figure 8a–e shows the 3D microstructures at hydration times of 10, 40, 180, 360, and 420 min. In these figures, the red, blue, and grey areas represent large macro-pores containing water, micropores containing water, and cement particles, respectively. Comparing Fig. 8a, b, it is observed that some new cement particles appear at points indicated by the arrows. It can be proved that some cement particles sink during the early stages of hydration. Comparing Fig. 8c–e, it is observed that macro-pores decreased in number and some new micropores appeared.

Figure 9 presents a cutaway of the 3D microstructure of 1# obtained using nano-CT. The microstructures are observed at hydration times of 180, 360, and 420 min. It can also be observed that with an increase in the hydration time, some hydration products fill the macro-pores, which can reduce the pore volume and form many micropores. The interaction between water and pore surface of the micropores is stronger than the interaction with macro-pores, which is disadvantageous in transmitting hydrostatic pressure in cement slurries. According to the discussion in Sects. 3.1 and 3.2, it can be understood that in stages II and III, the hydrostatic pressure in 1# is transmitted by pore water. The hydrostatic pressure in 1# in stage II is approximately equal to the hydrostatic pressure of water. However, the formation of hydration products cuts off the channels between particles, which reduces the hydrostatic column height (h) of free water in the pores and decreases hydrostatic pressure in the cement slurry.

3.4.2 Pore Structure in the Cement Slurry

The T_2 curves of 1# cement slurry at different hydration times are shown in Fig. 10; it can be seen that the T_2 of fresh cement slurry (hydration for 0 min) is distributed into two regions. The first region is distributed in the 4–30-ms range, and the second region is above 100 ms. According to Bede et al.'s (2016) report, in the fresh cement slurry, the main pores are macro-pores and capillary pores. In Fig. 8, two obvious changes can be seen. (1) With an increase in the hydration time, the T_2 curves of the cement slurry moved to the left. (2) At hydration times of 0, 60, and 120 min, the peak positions of the three T_2 curves were similar but their

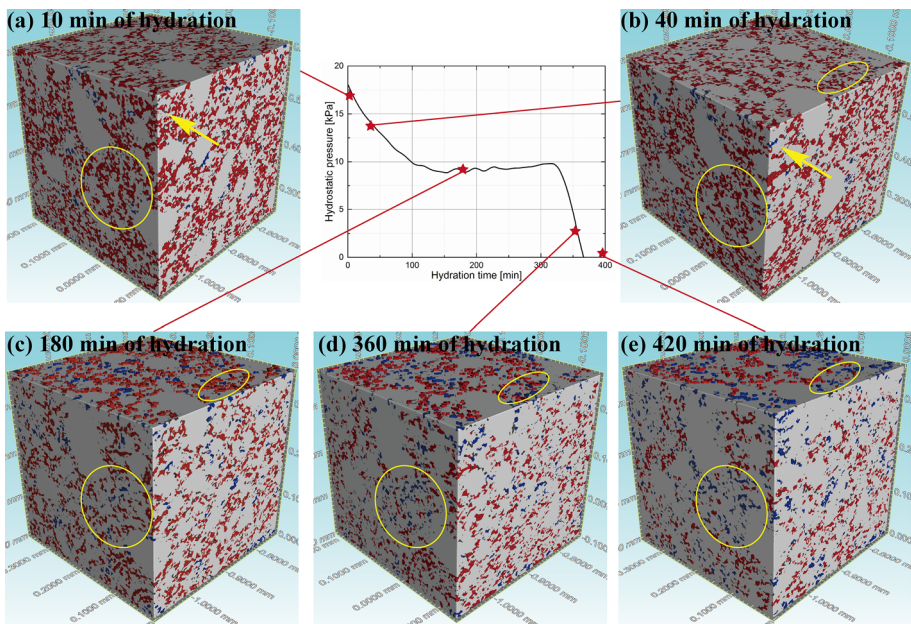


Fig. 8 Nano-CT analysed 3D microstructure of 1# at different hydration times. The red, blue, and grey areas represent large pores containing water, micropores containing water, and cement particles, respectively

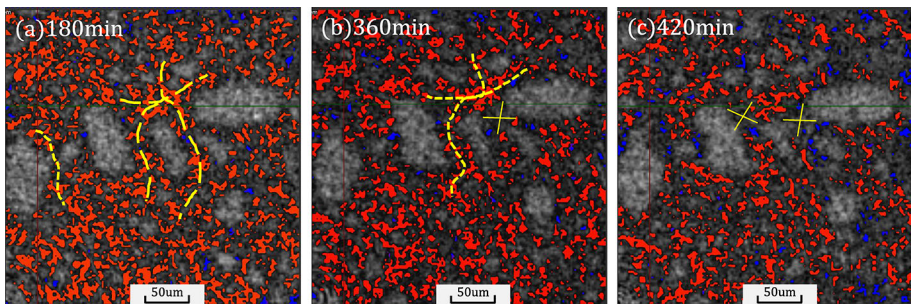


Fig. 9 Cutaway of the 3D microstructures of 1# generated using nano-CT

amplitudes were different; furthermore, when the hydration time is 300 min, the amplitudes of the T_2 curves of the cement slurry decreased once again.

Comparing the T_2 curves obtained at hydration times of 0 and 120 min (Fig. 10), it can be suggested that the particles of the fresh cement slurry (hydration for 0 min) are suspended to form uniform pores. Sedimentation of the cement particles (hydration for 120 min) widens the pore size range in the cement slurry, which in turn widens the range of the obtained T_2 curves. From the 3D microstructure results (shown in Fig. 8), it can be inferred that with an increase in the hydration time, some hydration products are formed between the cement particles, which changes the pore structure and decreases pore size. According to Eq. (2), this can be expressed in terms of the decrease in T_2 values.

The distribution of T_2 curves is related to the pore size. The peak area of the T_2 curve is related to the relative percentages of different types of pores. Figure 11 shows the changes

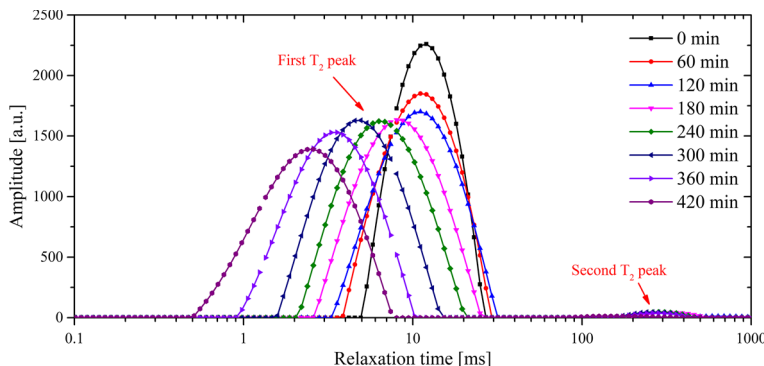


Fig. 10 Changes in the T_2 curves of the cement slurry 1# at different hydration times

in T_2 peak area when the hydration time is varied (shown in Fig. 11a) and the relationship between T_2 peak area and hydrostatic pressure of 1# (shown in Fig. 11b). From the results in Fig. 11, it can be understood that the relative percentage content of pores and hydrostatic pressure are linearly related to each other.

3.4.3 Microstructure of 1# Cement Slurry Using SEM

Figure 12 shows the microstructure of 1# in stages II and III. Figure 12a shows the microstructure of the cement particles, and Fig. 12b depicts the microstructure of 1# hydrated for 180 min. At this time, particles accumulation can be observed and the surfaces of the cement particles are covered by hydration shells. With an increase in the hydration time, the surfaces of the cement particles become rough and some hydration products start crystallizing and growing on the surfaces of the particles. These hydration products do not have a fixed shape and are porous (shown in Fig. 12d).

Meanwhile, some hydration products with fixed shapes start forming in the pores of the cement slurry (shown in Fig. 12e). Its size is increasing with the increase in hydration time, and when the hydration time is 420 min the pore is filled by the hydration products (shown as in Fig. 12f). Compared to the nano-CT images, the changes in the microstructure of the cement slurry can be more clearly presented using SEM. The hydration products of the cement slurry are porous and fill macro-pores. Further, a large number of micropores are formed during the hardening of the cement slurry, which leads to changes in the pore distribution.

According to the SEM results, the pores formed in the cement slurry at different hydration times can be divided into three types, including macro-pores, capillary pores, and gel pores (shown in Fig. 12). Bede et al. (2016) reported that $T_2 < 1.5$ ms is related to C–H–S gel pores, $1.5 < T_2 < 7.5$ ms indicates capillary pores, and $T_2 > 7.5$ ms implies macro-pores. Therefore, the relative percentage contents of different types of pores in the cement slurry at different hydration times are analysed. The results are shown in Fig. 13. It can be seen that in stages I and II of hydrostatic pressure reduction, mostly macro-pores and capillary pores are present in the slurry. Meanwhile, in stage III, the macro-pores rapidly change to capillary pores and some gel pores.

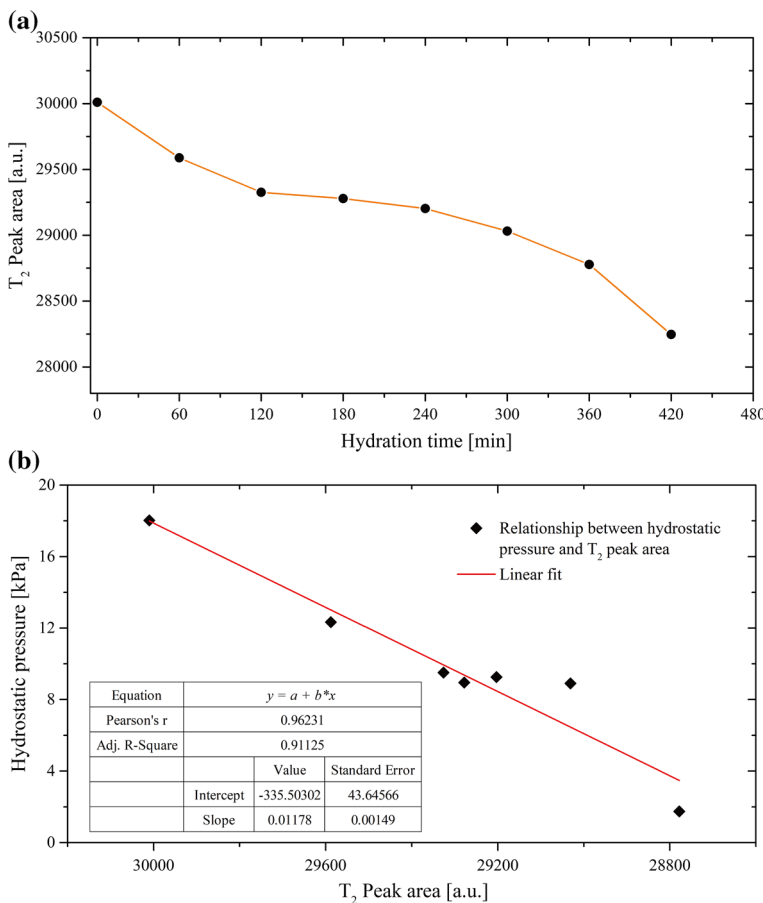


Fig. 11 Relationship between hydrostatic pressure and relative percentage content of pores. **a** Changes in T_2 peak area with hydration time and **b** relationship between hydrostatic pressure and T_2 peak area

3.5 Mechanism of Hydrostatic Pressure Reduction

The evolution of microstructure and the pore structure in a cement slurry are the key factors determining hydrostatic pressure reduction (Man and Jing 2000). In stage I of hydrostatic pressure reduction, due to sedimentation of the cement particles, the gravity force of the cement particles cannot be transmitted by hydrostatic pressure. At this time, the hydrostatic pressure of the cement slurry is approximately equal to the hydrostatic pressure of water. The hydration of cement particles is a dissolution and deposition process (Sobolkina et al. 2016). With an increase in the hydration time of the cement slurry, some cement particles are dissolved in the pore water and the density of the pore water is slightly increased, which induces a slight increase in the hydrostatic pressure of the cement slurry in stage II (as shown in Fig. 4).

In stages II and III, the hydrostatic pressure of 1# is transmitted by free water in the pores. In the cement slurry, the pores are filled with water. Therefore, depending on the pore size, the pore water can be distinguished as free water, capillary water, and gel water. Figure 14

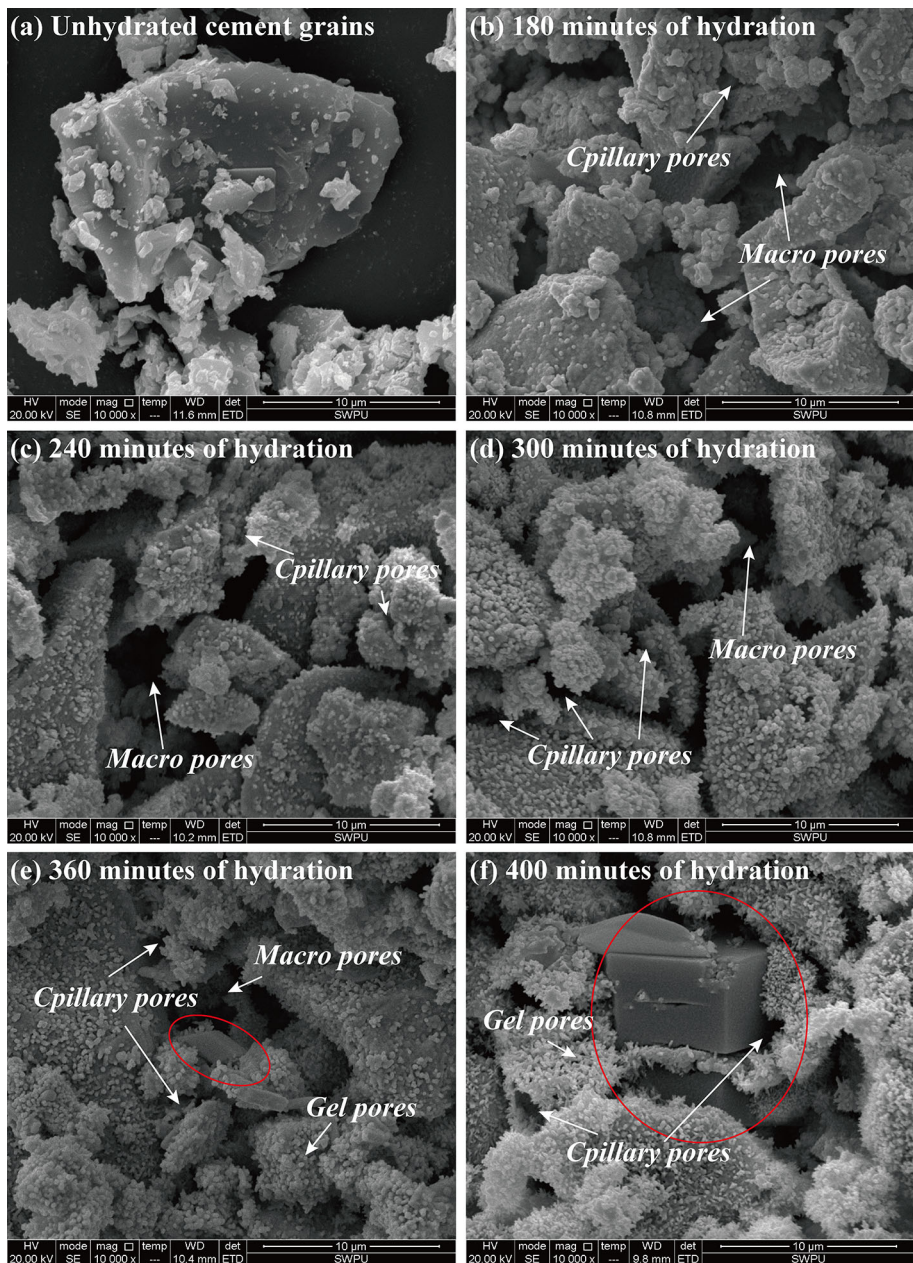


Fig. 12 Microstructures of the cement slurry 1# at different hydration times

depicts the evolution of microstructure and water distribution in the cement slurry. Due to the formation of hydration products and changes in the pore structure, free water is turned into capillary water and gel water. The interaction between capillary water, gel water, and pore surfaces is stronger than the interaction with free water. In addition, some hydration

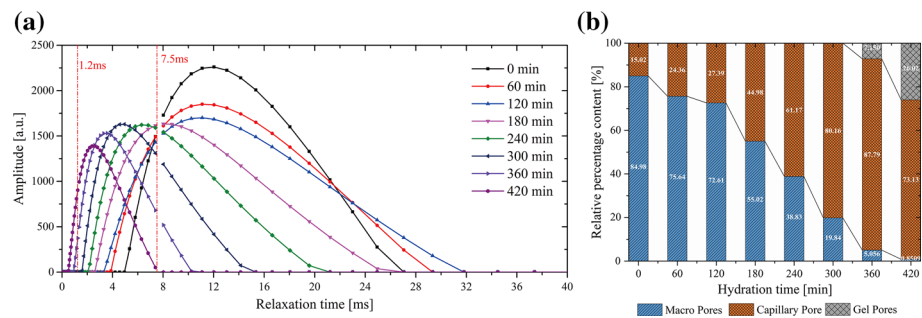


Fig. 13 Relative percentage content of pores in 1# at different hydration times. **a** Changes in the first T_2 peak and **b** relative percentage of pores

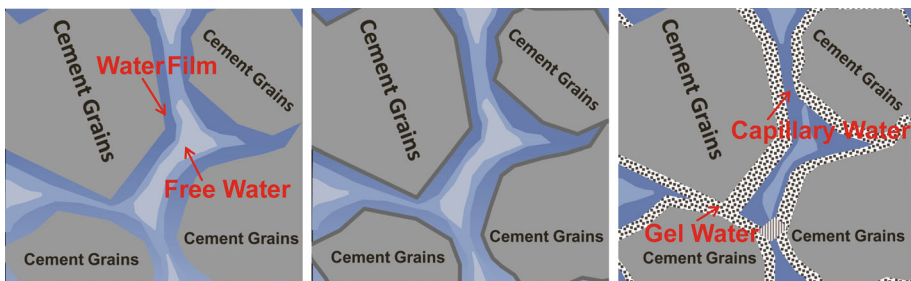


Fig. 14 Change in the microstructure and water distribution in a cement slurry

products are formed in the pores and fill them, which reduces the column height of the free water in the pores (h) (shown in Fig. 9). The hydrostatic pressure of the cement slurry is thus reduced. Meanwhile, because of the formation of hydration products between cement particles, physical bonding between the cement particles changes into chemical bonding, leading to an increase in the slurry strength.

4 Conclusions

The results presented in this study reveal that in the early hydration stages of a cement slurry, the transmission of hydrostatic pressure (in a fresh cement slurry) follows Pascal's law. However, because of the sedimentation of cement particles, the hydrostatic pressure of the slurry can only be transferred by the pore solution and the hydrostatic pressure of cement slurry is reduced. With an increase in the hydration time, the hydration reaction is accelerated and some hydration products are formed between the cement particles. Because of the formation of such products, some of which are porous, some macro-pores are filled with hydration products to form a number of micropores, which leads to most of the free water turning into capillary water and gel water. The interaction between capillary water, gel water, and micropores is stronger than that between free water and macro-pores, which leads to a reduction in the hydrostatic pressure of the cement slurry. Some hydration products are formed in the pores of the cement slurry, due to which the pores are filled. This also leads to a reduction in the height of the hydrostatic column and hydrostatic pressure of the cement slurry.

Acknowledgements The authors are grateful for the support provided by the National Key R&D Program of China (2016YFB0303600). And authors also would like to thank Advanced Cementing Materials Research Center of SWPU for the kind assistance in laboratory testing.

References

- American Petroleum Institute (API): API RP-10A, Specification for Cements and Materials for Well Cementing, 23rd edn. American Petroleum Institute Publishing Services, Washington (2002)
- American Petroleum Institute (API): 10B-2, Recommended Practice For Testing Well Cements, 2nd edn. American Petroleum Institute Publishing Services, Washington (2013)
- Angulo-Ramírez, D.E., Mejía de Gutiérrez, R., Puertas, F.: Alkali-activated Portland blast-furnace slag cement: mechanical properties and hydration. *Constr. Build. Mater.* **140**, 119–128 (2017). <https://doi.org/10.1016/j.conbuildmat.2017.02.092>
- Baumgarte, C., Thiercelin, M.J., Klaus, D.: Case studies of expanding cement to prevent microannular formation. In: Proceedings of SPE Annual Technical Conference and Exhibition (1999)
- Bede, A., Scurtu, A., Ardelean, I.: NMR relaxation of molecules confined inside the cement paste pores under partially saturated conditions. *Cem. Concr. Res.* **89**, 56–62 (2016). <https://doi.org/10.1016/j.cemconres.2016.07.012>
- Bernardes, E.E., Mantilla Carrasco, E.V., Vasconcelos, W.L., De Magalhães, A.G.: X-ray microtomography (μ -CT) to analyze the pore structure of a Portland cement composite based on the selection of different regions of interest. *Constr. Build. Mater.* **95**, 703–709 (2015). <https://doi.org/10.1016/j.conbuildmat.2015.07.128>
- Carter, G., Slagle, K.: A study of completion practices to minimize gas communication. *J. Pet. Technol.* **26**, 1170–1174 (1972). <https://doi.org/10.2118/3164-PA>
- Chung, S.Y., Elrahman, M.A., Stephan, D., Kamm, P.H.: Investigation of characteristics and responses of insulating cement paste specimens with Aer solids using X-ray micro-computed tomography. *Constr. Build. Mater.* **118**, 204–215 (2016). <https://doi.org/10.1016/j.conbuildmat.2016.04.159>
- Dalas, F., Korb, J.-P., Pourchet, S., Nonat, A., Rinaldi, D., Mosquet, M.: Surface relaxivity of cement hydrates. *J. Phys. Chem. C* **118**, 8387–8396 (2014). <https://doi.org/10.1021/jp500055p>
- Dusterhoff, D., Wilson, G., Newman, K.: Field study on the use of cement pulsation to control gas migration. Presented at the (2002)
- Hou, T.C., Nguyen, V.K., Su, Y.M., Chen, Y.R., Chen, P.J.: Effects of coarse aggregates on the electrical resistivity of Portland cement concrete. *Constr. Build. Mater.* **133**, 397–408 (2017). <https://doi.org/10.1016/j.conbuildmat.2016.12.044>
- Ji, Y., Sun, Z., Yang, X., Li, C., Tang, X.: Assessment and mechanism study of bleeding process in cement paste by 1H low-field NMR. *Constr. Build. Mater.* **100**, 255–261 (2015). <https://doi.org/10.1016/j.conbuildmat.2015.09.062>
- Joseph, S., Bishnoi, S., Van Balen, K., Cizer, Ö.: Modeling the effect of fineness and filler in early-age hydration of tricalcium silicate. *J. Am. Ceram. Soc.* **100**, 1178–1194 (2017). <https://doi.org/10.1111/jace.14676>
- Kim, K.Y., Yun, T.S., Choo, J., Kang, D.H., Shin, H.S.: Determination of air-void parameters of hardened cement-based materials using X-ray computed tomography. *Constr. Build. Mater.* **37**, 93–101 (2012). <https://doi.org/10.1016/j.conbuildmat.2012.07.012>
- Lanzón, M., Cnudde, V., De Kock, T., Dewanckele, J.: X-ray microtomography (μ -CT) to evaluate microstructure of mortars containing low density additions. *Cem. Concr. Compos.* **34**, 993–1000 (2012). <https://doi.org/10.1016/j.cemconcomp.2012.06.011>
- Li, Z., Vandebossche, J., Iannacchione, A., Brigham, J., Kutchko, B.: Theory-based review of limitations with static gel strength in cement/matrix characterization. *SPE Drill. Complet.* **31**, 145–158 (2016). <https://doi.org/10.2118/178923-PA>
- Lothenbach, B., Winnefeld, F., Alder, C., Wieland, E., Lunk, P.: Effect of temperature on the pore solution, microstructure and hydration products of Portland cement pastes. *Cem. Concr. Res.* **37**, 483–491 (2007). <https://doi.org/10.1016/j.cemconres.2006.11.016>
- Man, H.N., Jing, X.D.: Pore network modelling of electrical resistivity and capillary pressure characteristics. *Transp. Porous Media* **41**, 263–286 (2000). <https://doi.org/10.1023/A:1006612100346>
- Marchon, D., Flatt, R.J.: Mechanisms of cement hydration. In: Science and Technology of Concrete Admixtures, pp. 129–145 (2015)
- McDonald, P.J., Rodin, V., Valori, A.: Characterisation of intra- and inter-C-S-H gel pore water in white cement based on an analysis of NMR signal amplitudes as a function of water content. *Cem. Concr. Res.* **40**, 1656–1663 (2010). <https://doi.org/10.1016/j.cemconres.2010.08.003>

- Newman, K., Wojtanowicz, A., Gahan, B.C.: Cement pulsation improves gas well cementing. *World Oil*. **222**, 89–94 (2001)
- Prohaska, M., Ogbe, D.O., Economides, M.J.: Determining wellbore pressures in cement slurry columns. In: Western Regional Meeting, pp. 407–412. Society of Petroleum Engineers, Anchorage, Alaska (1993)
- Sabins, F.L., Services, H.: Transition time of cement slurries between the fluid and set states. *SPE J.* **22**, 875–882 (1982)
- Schock, J., Liebl, S., Achterhold, K., Pfeiffer, F.: Obtaining the spacing factor of microporous concrete using high-resolution dual energy X-ray micro CT. *Cem. Concr. Res.* **89**, 200–205 (2016). <https://doi.org/10.1016/j.cemconres.2016.08.008>
- Skibsted, J., Andersen, M.D.: The effect of alkali ions on the incorporation of aluminum in the calcium silicate hydrate (C–S–H) phase resulting from Portland cement hydration studied by ^{29}Si MAS NMR. *J. Am. Ceram. Soc.* **96**, 651–656 (2013). <https://doi.org/10.1111/jace.12024>
- Sobolkina, A., Mechtcherine, V., Bergold, S.T., Neubauer, J., Bellmann, C., Khavrus, V., Oswald, S., Leonhardt, A., Reschetilowski, W.: Effect of carbon-based materials on the early hydration of tricalcium silicate. *J. Am. Ceram. Soc.* **99**, 2181–2196 (2016). <https://doi.org/10.1111/jace.14187>
- Sutton, D.L., Faul, R., Sabins, F.: Annular gas flow theory and prevention methods described. *Oil Gas J. (United States)* **82**, 50 (1984)
- Zhang, X.: Study on Weightlessness Mechanisms of Slurry Suspension during Cement Gelation. PhD dissertation. Southwest Petroleum University, Sichuan, China (2002)